Selectively exciting quasibound states in the continuum in open microwave resonators using dielectric scatters

Olugbenga Gbidi and Chen Shen

Phys. Rev. B **107**, 184309 — Published 22 May 2023

DOI: 10.1103/PhysRevB.107.184309

Selectively Exciting Quasi-Bound States in the Continuum in Open Microwave Resonators Using Dielectric Scatters

Olugbenga Gbidi and Chen Shen*

Department of Mechanical Engineering, Rowan University, Glassboro, NJ 08028, USA

shenc@rowan.edu

Abstract:

Bound states in the continuum (BICs) are wave modes that remain in the continuous spectrum of radiating waves that carry energy, however, remain perfectly localized and non-radiating. BICs, or embedded eigenmodes, exhibit high quality factors that have been observed in optical and acoustic waveguides, photonic structures, and other physical systems. However, there are limited means to manipulate these BICs in terms of the quality factor and their excitation. In this work, we show that quasi-BICs (QBICs) in open resonators can be tailored by introducing embedded scatters. Using microwave cavities and dielectric scatters as an example, QBICs are shown capable of being repeatedly manipulated by tuning the geometry of the structure and the specific locations of the dielectric scatters. Using coupled mode theory (CMT) and numerical simulations, we demonstrate by altering dielectric and structural parameters, tuning the quality factor as well as selective excitation and suppressing of specific QBIC modes can be achieved. These results provide an alternative means to control BICs in open structures and may be beneficial to applications including sensors and high-*Q* resonators that need confined fields and selectivity in frequency.

I. INTRODUCTION

Bound states in the continuum (BICs) were first proposed and mathematically proven by John von Neumann and Eugene Wigner in quantum systems in the 1920s [1]. BICs are known to be embedded eigenstates, trapped modes, or waves in a system where the energy lies in the continuous spectral range of radiating waves but remain perfectly localized [2,3]. The difference between BICs and leaky resonances is that they lie within the spectrum corresponding to the continuum but do not radiate any energy, which indicates they maintain an infinitely long lifetime. Theoretically, the quality factor approaches infinity for ideal BICs since the energy is completely trapped. This peculiar phenomenon has been observed in different physical systems such as photonics and optics [4–14], acoustic waves [15–19], water waves [16,20–23], and in recent years the microwave regime [24–27]. Since BICs are ideal dark modes that remain in the continuum, the imaginary part of their complex eigenfrequency vanishes, and an exceptionally high Q factor is sustained. Recent studies have shown that resonators, either single or multiple, can support different types of BICs with high Q-factors through symmetry protection, parameter tuning, or accidental field localization from non-symmetric structures [8,11,28,29]. BICs demonstrated so far include the symmetry-protected (SP) BICs [13,17,29,30], Friedrich-Wintgen (FW) BICs [17,18,26,29,31], Fabry-Perot (FP) BICs [4,8,18,32–34], accidental BICs [29,35–37], among others, according to their physical mechanisms. For example, SP BICs are localized in structures due to the orthogonality of the eigenmodes to the propagating modes and FW BICs are supported by the destructive interference of the resonant modes. FP BICs, on the other hand, emerge when two identical resonators are coupled to each other and the propagating phase is tailored. Structures have also been shown to support resonance states with suppressed Q-factors because of material absorption, symmetry breaking, structural disorder, as well as the interaction with propagation modes [38,39]. These states are often termed as quasi-BICs (QBICs) where radiation is present but high Q factors are still maintained.

In recent years, researchers have demonstrated and observed BICs and QBICs in different systems and the associated phenomena. Their unique properties have led to potential applications including but not limited to waveguides, lasers, sensors, and filters. For example, guided resonance modes with enhanced Q-factors and suppressed out-of-plane scattering can be excited by merging multiple BICs which carry topological charges [40]. Unidirectional resonances that radiate towards only one side of the structure are further realized by manipulating the topological charges carried by the BICs [41]. Chiral BICs and QBICs, on the other hand, enable new opportunities for the control of different polarization states which could find applications in chiral sensing, detection, and so on [42–44]. BICs have also been found useful in lasers with reduced linewidth, out-of-plane losses, and improved robustness and scalability [12,45,46]. In acoustics, BICs and QBICs have found applications in perfect absorption, emission enhancement, and so on [47–49].

Despite the rapid development in this field, effective approaches to manipulate or excite certain modes of BICs or QBICs remain scarce. The goal of this paper is to study the interaction between resonant cavities and embedded scatters and leverage such interactions for the manipulation of QBICs. An open microwave cavity resonator attached to a waveguide is constructed as an example to illustrate the concept. We find that placing dielectric scatters within the cavity can lead to the suppression or enhancement of specific modes depending on their symmetry with respect to the original modes. Furthermore, at specific geometric conditions, the introduction of the scatters can suppress one mode while being able to maintain another. In this manner, selective excitation of a certain mode is achieved which leads to the control of the modes in a versatile way. These findings provide a useful means to tune the properties of QBICs as well as the selective excitation of certain modes by exploiting the symmetry and wave-matter interaction in open systems.

II. MODEL AND THEORY

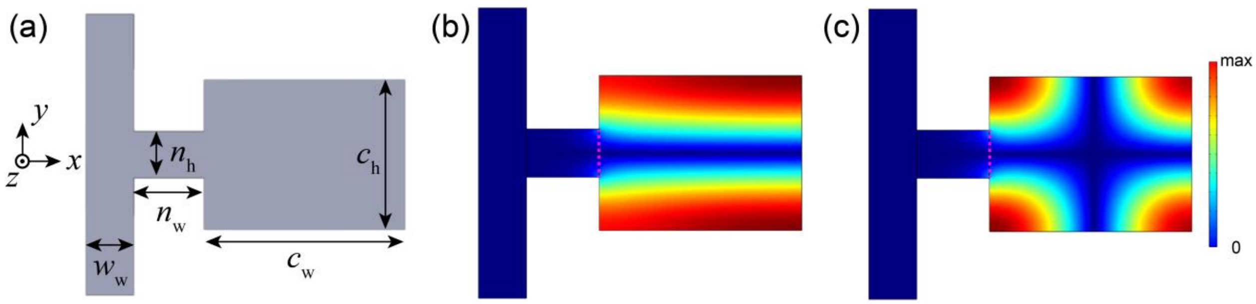

Figure 1. QBICs in an open microwave resonator. (a) The geometric configuration of the resonator. (b) and (c) The magnetic field distribution of the TM_{12} mode and TM_{22} mode inside the structure without scatters, respectively.

Here we consider TM-polarized microwave propagation in the GHz regime. Figure 1 depicts the proposed structure in this study which contains a 2D open resonator attached to a waveguide with air as the background medium. Each of the boundary walls in the structure is a perfect electrical conductor (PEC) with the ends of the waveguide being the input and output ports, respectively. The original geometry dimensions start with the waveguide's width $w_w = 20$ mm and height $w_h = 120$ mm. The connecting neck has a width of $n_w = 30$ mm and height of $n_h = 20$ mm. The cavity's width and height are $c_w = 86$ mm and $c_h = 64$ mm, respectively. Figures 1(b-c) depict the magnetic field strength (H_z component) at two representative eigenfrequencies. These are found to be QBICs by the symmetric conditions of their eigenfields and the obtained Q-factors are

5.1886×10^6 and 2.086×10^6, respectively. They are labeled as the TM_{12} and TM_{22} modes based on the number of maxima in the magnetic field distributions in the *x*- and *y*-axes, respectively.

The characteristics of these QBICs can be analyzed by the scattering properties of the resonators by exciting the external ports. A plane wave solution to the wave equation can be found in an electric field with only an x component and no variation in the *x*- and *y*-directions [50]. The reduced Helmholtz equation considers propagation in the *z*-direction. Theoretically, the resonator-waveguide structure can be described by the scalar wave function $\psi_m(x,y)$ which describes the H_z component obeying the Helmholtz equation: $\hat{H}\psi_m(x,y)=\frac{\omega_m^2}{c^2}\psi_m(x,y)$, where $\hat{H}=\nabla^2+\frac{\omega_m^2}{c^2}\left[n^2(x,y)+1\right]$ is the Hamiltonian, ω is the frequency, and c is the light speed [27]. $n(x,y)$ is the refractive index which can be spatially varying when scatters are introduced. To estimate the quality factor of the cavity, the reflection coefficient obtained from the coupled mode theory (CMT) is studied to help verify the existence of the QBICs [17,51]:

$$R=\frac{(\omega-\omega_0)^2\cos^2\theta+\gamma^2\sin^2\theta\mp2\sin\theta\cos\theta(\omega-\omega_0)\gamma}{(\omega-\omega_0)^2+\gamma^2} \tag{1}$$

Here ω_0 is the resonance frequency, γ is the decay rate, and θ is the phase angle of the eigenfrequency. To apply the CMT, an eigenvalue study based on the finite element method using COMSOL Multiphysics is first carried out to obtain the quality factor of the QBIC, which is done by relating the real and imaginary parts of the complex eigenfrequencies, $\omega=\omega_0-i\gamma$ via $Q=\frac{\omega_0}{2\gamma}$. The obtained resonance frequency and decay rate from the eigenvalue study are then inserted into Eq. (1) to retrieve the reflection coefficient by fitting the phase angle. The results are summarized in Fig. 2, with fitting parameters $\gamma=2.28\times10^{-7}i$ and $\theta=0.40\pi$ in Fig. 2(a) and $\gamma=7.08\times10^{-7}i$

and $\theta = 0.23\pi$ in Fig. 2(b). In the meantime, numerical simulations are carried out to validate the theoretical model. In COMSOL, one port is used as the input and the reflection coefficient is recorded. Good agreement is observed between the analytic model and numerical simulations for both modes. This indicates that the model captures the scattering properties of the cavity and provides an efficient way to model QBICs. The reflection coefficient shown in Fig. 2 features a Fano resonance with an asymmetric lineshape. The Fano resonance curve displays the interference between the bright mode and the dark mode of the scattering events: the radiation continuum and the eigenmode of the cavity [26]. For the QBIC studied here, the *Q*-factors are very high, therefore the bright mode exhibits an almost flat line within the frequency of interest. On the other hand, the fact that these bound states are visible in the scattering spectrum and can be excited from the far field also confirms they are QBICs.

Since the energy is mostly trapped within the cavity and not radiating into the main waveguide, the magnetic field distribution at the neck must be symmetric so that it cancels out. To confirm this, cutline plots are taken along the neck connecting to the waveguide as illustrated by the magenta dotted lines in Figs. 1(b-c) to measure the magnetic field. The results are illustrated in Fig. 2(c) where it is found that the normalized magnetic field strength at the neck exhibits symmetric distributions, demonstrating the existence of SP QBICs.

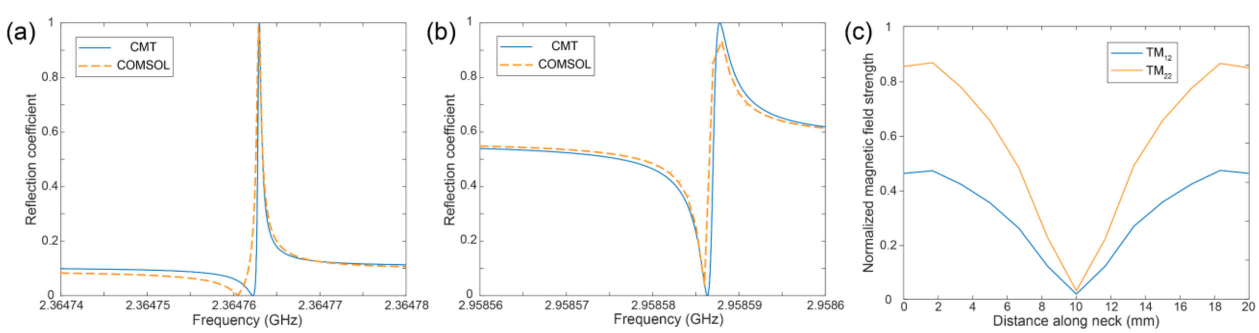

Figure 2. Verification of the QBICs by the scattering property calculations using CMT and COMSOL simulations for the no scatter case. (a) The reflection spectrum of the TM_{12} mode. (b) Reflection spectrum the TM_{22} mode. (c) Normalized magnetic field strength along the neck for the TM_{12} and TM_{22} modes. A symmetric field distribution is observed.

III. RESULTS AND DISCUSSION

To begin, the cavity's width and height are changed to study the dependence of the quality factor of the QBICs on the geometrical parameters of the cavity. The *Q*-factors are calculated based on the eigenfrequency study outlined above and the results are summarized in Fig. 3. We vary one parameter while fixing the others to tune the geometry and observe the variation of the *Q*-factors of QBICs. First, the width of the cavity is varied, and the results are shown in Fig. 3(a). By incrementally increasing the cavity, the *Q*-factors of the bound states increase for both modes. In Fig. 3(b), an increase in the cavity's height leads to a similar trend for the *Q*-factors for both modes. Specifically, faster growth of the *Q*-factors is seen for the TM_{12} mode as the width of the cavity is increased.

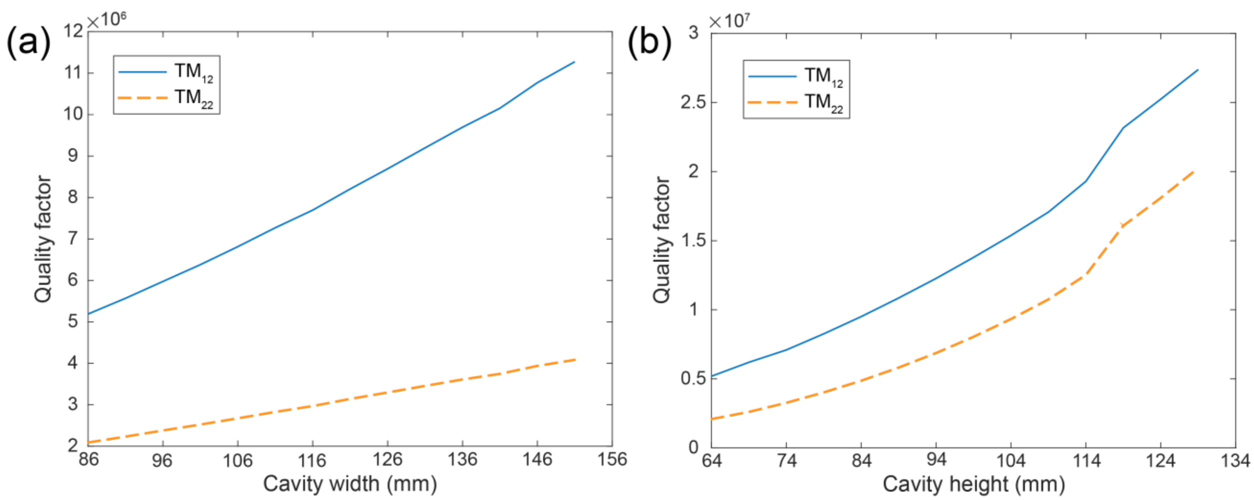

Figure 3. Influence of the cavity size on the Q-factors of the QBICs in the open microwave resonator. (a) The effects on the *Q*-factors by extending the cavity width. (b) The effects on the *Q*-factors by extending the cavity height.

On the other hand, the frequency of both TM_{12} and TM_{22} modes decreases as the cavity width increases, which is evidenced by the redshift of Fano resonances in Fig. 4 and aligns with the trend for standard cavities when their size changes. Higher *Q*-factors are manifested by the sharper asymmetric peak of Fano resonance at lower frequencies. The results demonstrate how the dimensions of the cavity can impact the *Q*-factors of the structure. A recent study discusses the importance of the symmetry of the entire structure and the size ratio of the cavity that can affect the *Q*-factors of the induced BICs [17]. Similar trends are found here for the open microwave resonator.

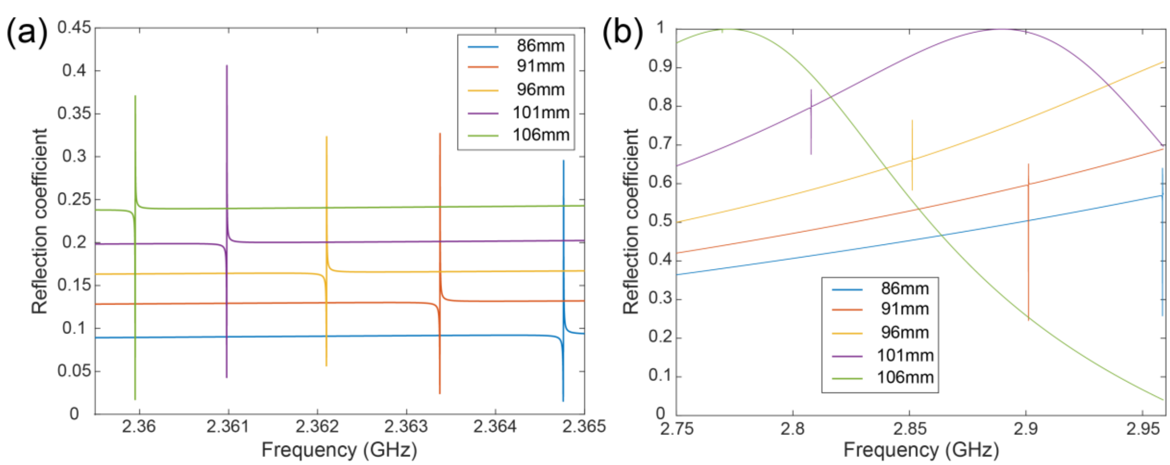

Figure 4. The reflection spectrum of the resonator when excited from the external port with various cavity widths. (a) Fano resonance plot of the TM_{12} mode. (b) Fano resonance plot of the TM_{22} mode.

Next, we move to incorporate dielectric scatters into the structure to study their effects on the BICs. The dielectric scatters have a circular cross section with radius r_d being 10 mm and are made of Teflon. In the simulations, the Teflon has a relative permeability of 1, relative permittivity of 2.1, and electrical conductivity of 1×10^{-25} S/m. Previously, dielectric scatters have been proposed to manipulate BICs in resonator structures [24,27]. These dielectric scatters alter the field distribution by interacting with the structures or causing scattering effects. While studies have shown that the scatters would not affect the BICs in a zero-index material (ZIM) [27], in this work we focus on the interactions between the scatters and the host resonator. We begin with single dielectric scatters positions at the corners of the cavity and the results are summarized in Fig. 5. It should be noted that only select cases of scatters at the top corners are shown, and identical results are seen in their bottom counterparts. When the dielectric scatters are introduced, the field distribution inside the cavity is altered, as shown in Figs. 5(a-d). For example, the magnetic field has a larger intensity near the rods, and its symmetry about the *x*-axis is broken. Notably, the degree of symmetry suppression depends on the location of the scatters. For example, the TM_{12} mode maintains higher *Q*-factors when the rods are located further away from the neck as depicted in Fig. 5(b). On the contrary, the TM_{22} mode has higher *Q*-factors when the rods are close to the neck, shown in Fig. 5(c). In all these cases, a dramatic decrease in the *Q*-factors is observed, which can be explained by the fact that the locations of the scatters break the original symmetry of the QBICs. The dielectric scatters redistribute the magnetic fields and lead to higher radiation leakage and lower *Q*-factors. The reflection spectrum exhibits a close approximation between numerical simulations and the CMT when the dielectric rods are in the top right corner of the cavity, as shown in Figs. 5(e-f). Here $\gamma = 1.30\times10^{-5} i$, $\theta = 0.60\pi$ and $\gamma = 8.04\times10^{-4} i$, $\theta = 0.74\pi$ are used for the two modes, respectively. A decrease of the *Q*-factors in both cases is clearly seen because of the symmetry of the field is broken. This is also confirmed by the cutline plot of the magnetic field in Figs. 5(g-h), where a non-symmetric field distribution at the neck is observed. As a result, more radiation leaks out from the cavity and the energy become less confined.

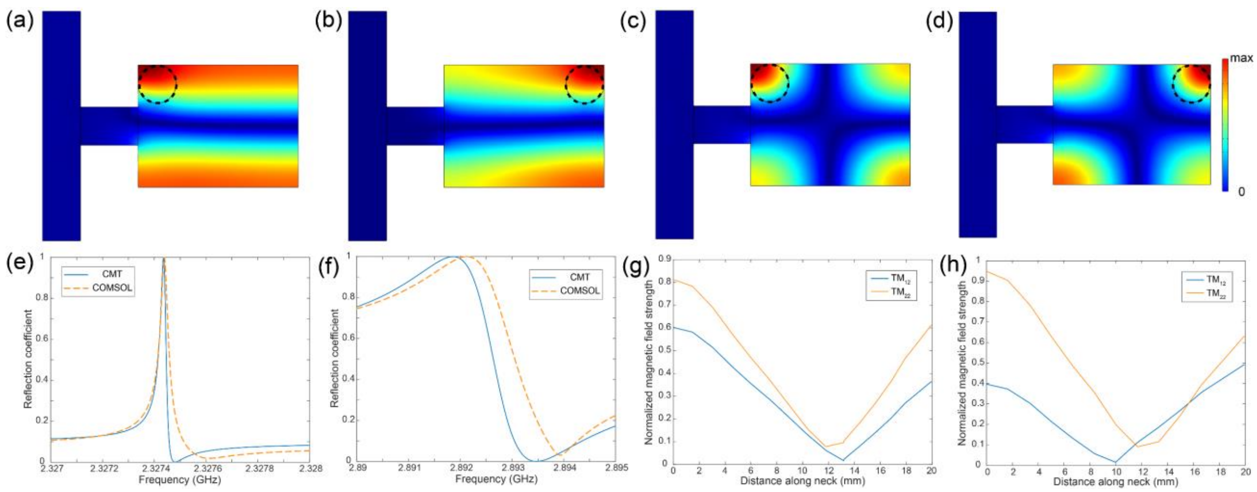

Figure 5. Effect of a single dielectric scatter on the QBIC in the open microwave resonator. (a) and (b) Magnetic field strength distribution of TM_{12} modes with dielectric scatters at the top left and top right corner of the cavity, respectively. (c) and (d) Magnetic field strength distribution of TM_{22} modes with dielectric rods at the top left and top right corner of the cavity, respectively. (e) and (f) The reflection spectrum of the TM_{12} and TM_{22} modes when excited from the external port. The dielectric scatters are placed at the top right corner of the cavity. (g) Normalized magnetic field strength along the neck for the TM_{12} and TM_{22} modes when the dielectric scatters are at the top left and top right corner of the cavity, respectively. The field distribution is no longer symmetric, which leads to the suppression of the QBICs.

To illustrate the relation between the symmetry conditions of the scatters and the QBICs, another dielectric rod is added symmetrically to the bottom of the cavity so that the two scatters are symmetric with respect to the *x*-axis. The corresponding magnetic fields are depicted in Figs. 6(a-f) where the dielectric rods are positioned in the left, center, and right of the cavity for the TM_{12} and TM_{22} modes, respectively. In this way, the locations of the scatters respect the symmetry of the QBICs (i.e., mirror symmetry about the *x*-axis). Consequently, the field distribution is not strongly disturbed, and these modes are maintained. The corresponding *Q*-factors variations are shown in Fig. 6(g) when the scatters are moved across the cavity. The quality factor of the TM_{12} mode increases from 5×10^6 to 7×10^6 while the TM_{22} mode fluctuates in the range between 2×10^6 and 3×10^6. As evidenced by the relatively high *Q*-factors, both QBICs are robust to the introduction of symmetrically loaded scatters. The slight increase in the *Q*-factors for the TM_{12} mode may be explained by the field localization to the right side of the cavity and hence less radiation occurs near the neck. The same trend is also captured by the theoretical calculations using CMT as illustrated in Figs. 7(a-f), where good agreement is observed with numerical simulations. Specifically, the following fitting parameters are used in each case: $\gamma = 2.23\times10^{-7}i$, $2.04\times10^{-7}i$, $1.52\times10^{-7}i$ and $\theta = -0.59\pi$, -0.62π, -0.33π for the TM_{12} mode; $\gamma = 4.38\times10^{-7}i$, $5.86\times10^{-7}i$, $2.85\times10^{-7}i$ and $\theta = 0.24\pi$, 0.27π, 0.25π for the TM_{22} mode.

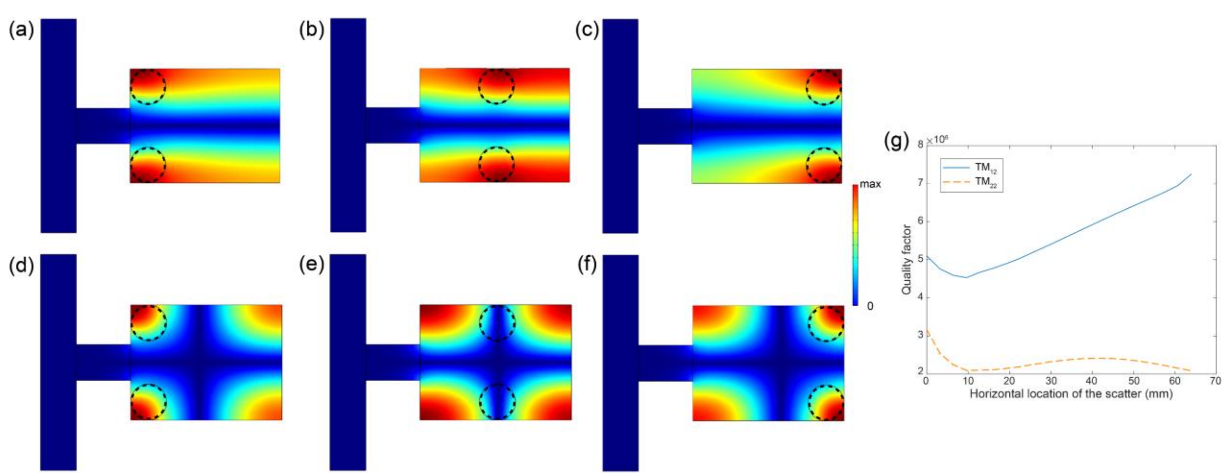

Figure 6. (a-c) Magnetic field distributions of the TM_{12} mode with symmetrically loaded dielectric scatters in the left, center, and right of the cavity, respectively. (d-f) Magnetic field distributions of the TM_{22} mode with symmetrically loaded dielectric scatters in the left, center, and right of the cavity, respectively. (g) The trend of Q-factors by changing the horizontal location of the scatters.

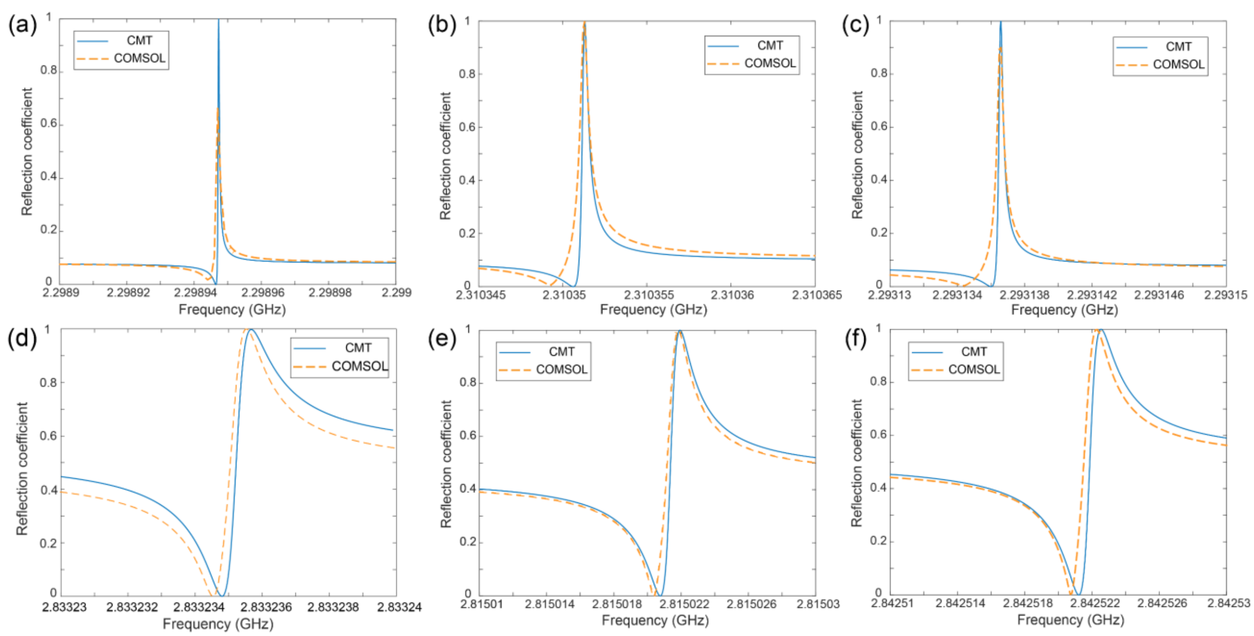

Figure 7. Reflection spectrum showing the Fano resonance plots by varying the horizontal location of a pair of symmetrically loaded dielectric scatters. (a-c) The dielectric scatters are positioned at the left, center, and right corners of the cavity, respectively for the TM_{12} mode. (b-f) The dielectric scatters are positioned at the left, center, and right corners of the cavity, respectively for the TM_{22} mode.

To gain more insight into the interaction between the scatters and the QBICs, the dielectric rods are placed asymmetrically and occupy opposite corners of the cavity. The magnetic field distributions in Fig. 8 show that the fields are generally distorted for both modes and the QBICs are suppressed. This is possibly caused by the locations of the scatters which are asymmetric and do not respect the symmetry of the QBICs, similar to the case of single scatters. The demonstration indicates the scatters can suppress certain modes if they do not obey the original field symmetry. However, when the dimensions of the cavity are altered, there are special situations where the QBICs are supported. To confirm this, the cavity's width and height are separately changed while the dielectric rods are still located in opposite corners. In Fig. 9(a), the plot of the *Q*-factors versus cavity height suggests that both the TM_{12} and TM_{22} modes are suppressed when the scatters are introduced, as evidenced by the decrease of the *Q*-factors compared to the no scatter case. This could be explained by the fact that the locations of the scatters do not respect the original symmetry of the QBIC modes, which generally leads to more energy leakage and hence a greater decay rate. On the other hand, the TM_{12} mode is more robust to the introduction of scatters while the *Q*-factors for the TM_{22} mode drop to a magnitude of 10^3. Interestingly, a peak is observed when $c_\mathrm{h} = 69$ mm for the TM_{12} mode. This indicates that this mode can still be excited with the existence of the scatters. In other words, it is possible to selectively excite the TM_{12} mode by introducing a pair of asymmetrically loaded scatters under a specific geometrical condition.

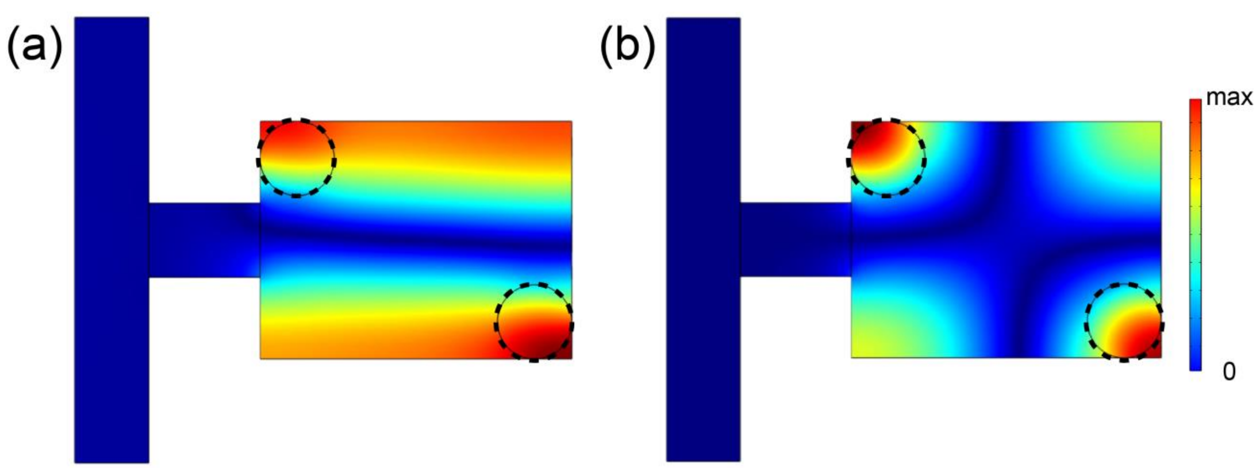

Figure 8. Magnetic field distributions of the (a) TM_{12} mode and (b) TM_{22} mode with two dielectric scatters positioned at the opposite corners inside the cavity.

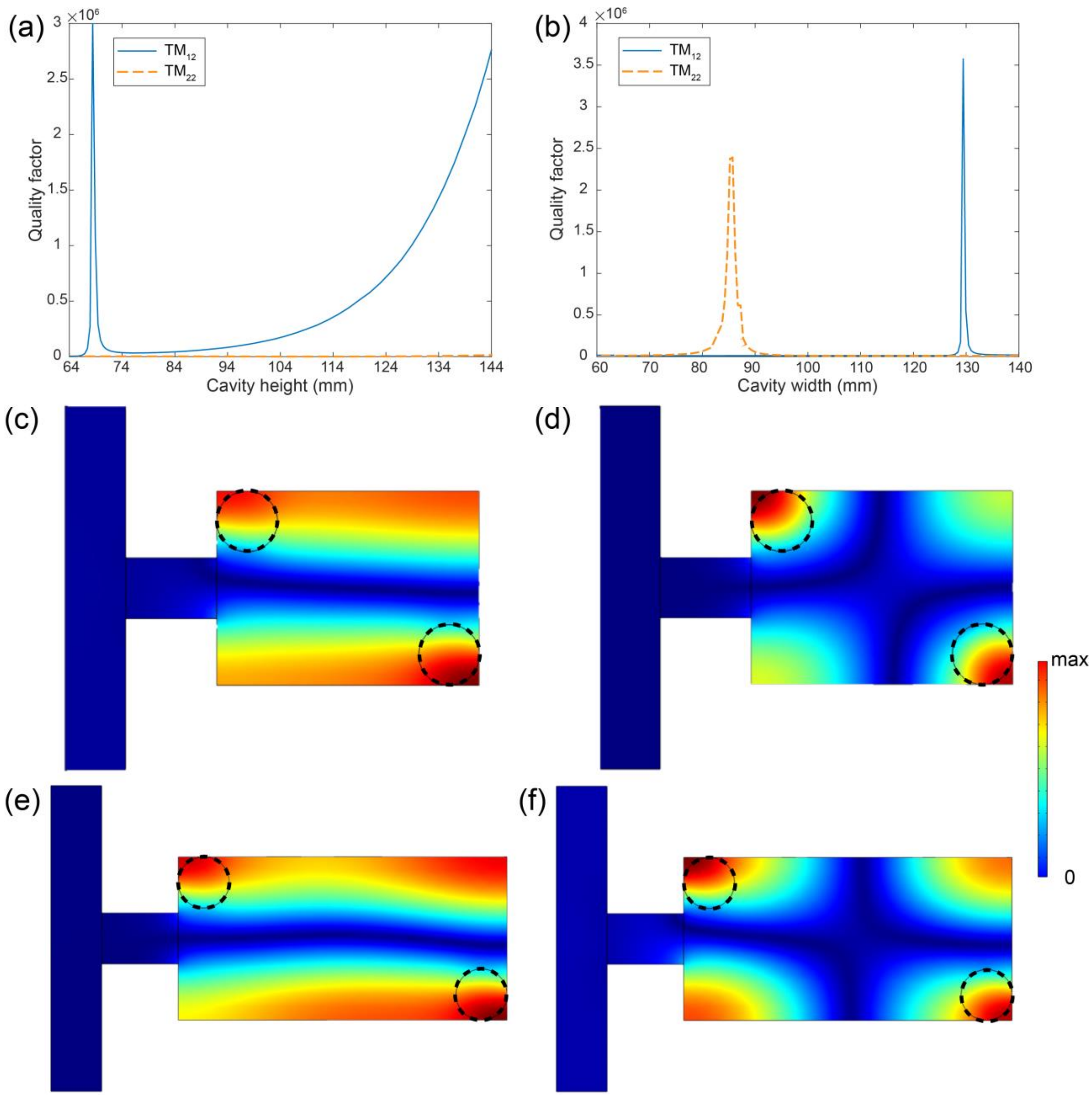

Figure 9. Variation of the Q-factors by varying the (a) height and (b) width of the cavity. The peaks in the Q-factors plot indicate that at specific geometric conditions, certain QBIC modes can be excited while other modes are suppressed when the scatters are placed asymmetrically in

the cavity. (c-d) The corresponding magnetic field distribution with a cavity width of 86 mm for the TM_{12} and TM_{22} modes, respectively. (e-f) The corresponding magnetic field distribution with a cavity width of 129 mm for the TM_{12} and TM_{22} modes, respectively.

Fig. 9(b) plots the change in the Q-factors of the QBICs as a function of cavity width. The trend reveals that like cavity height, the cavity width can be tuned to achieve better Q-factors for certain modes. By extending c_w , different modes are amplified at specific widths. Clearly, there is a dependence on the size ratio of the cavity when the modes can be selectively excited. This implies the symmetry conditions of the scatters and their interplay with the open resonators can be harnessed for the manipulation of SP BICs. The magnetic field distribution is further shown in Figs. 9(c-d) with a cavity width of 86 mm, where selective tuning of the QBICs is observed. Despite the same scatter locations, the field distribution for the TM_{12} mode is distorted but the TM_{22} mode maintains clear symmetry near the neck region. In Figs. 9(e-f), the field distributions at $c_w = 129$ mm illustrate the distribution of magnetic fields, where the symmetry of the fields is reversed. The TM_{12} mode is maintained and yields higher Q-factors while the TM_{22} mode is suppressed. Therefore, it is possible to selectively excite QBIC modes by carefully tailoring the dimension of the cavity so that the radiation cancellation at the neck is maintained. To verify the results, the normalized magnetic field strength at the neck is given in Figs. 10(a-b), where the cutline plots show that symmetry is clearly manifested for specific QBIC modes as they are selectively excited. The results suggest rich physics in controlling the properties of SP BICs by exploiting their symmetry and interaction with embedded scatters, which has also been demonstrated by recent studies. [52,53].

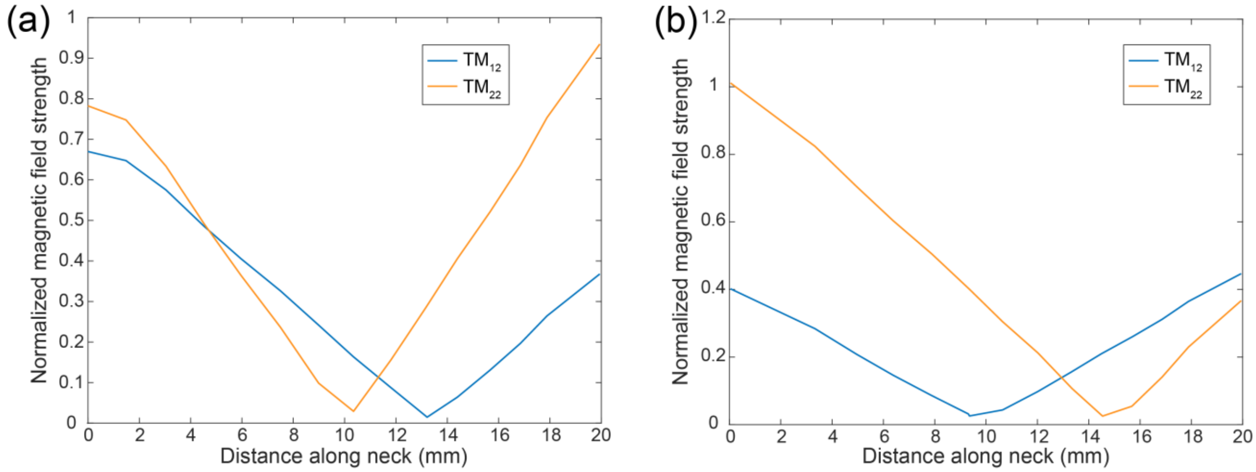

Figure 10. Normalized magnetic field strength along the neck for the TM_{12} and TM_{22} modes with a cavity width of (a) 86 mm and (b) 128 mm.

IV. CONCLUSION

BICs have emerged as a unique platform for the realization of high-*Q* resonance as well as other intriguing phenomena for novel wave-based devices. In this work, we study the interaction between SP QBICs and dielectric scatters in open microwave resonators. The QBIC modes are first studied, and the dependence of *Q*-factors on the geometry of the resonators is discussed. When dielectric scatters are introduced in the cavity, it is found that the interplay between the symmetric conditions of the scatters and the QBIC modes can have certain impacts. Specifically, when the locations of the scatters respect the symmetry of the corresponding QBIC modes, these modes are maintained, and the *Q*-factors can be tuned by changing the location of the scatters. When the scatters are not loaded according to the original symmetry of the QBICs, these modes are usually suppressed. However, in certain geometric conditions (e.g., with a specific aspect ratio of the cavity), one mode can still be excited while the others are absent. In the example we show here, the TM_{12} and TM_{22} modes can be selectively excited with different cavity widths. The results suggest the QBICs can be manipulated by leveraging the interaction between scatters and the corresponding modes. The ability to selectively excite or suppress certain modes is also desired in applications where a specific QBIC mode needs to be engineered. The main findings in this work may be verified with measurements based on physical structures at microwave frequencies. While the current work focuses on SP QBICs and rectangular cavities, it is envisioned that similar effects could also be found for other shapes such as cylindrical and spherical resonators as well as other modes, including FP and accidental BICs. It is hoped that this work will provide an alternative way to manipulate BICs including their *Q*-factors and the excitation of certain modes.

Acknowledgments

This work is supported by the National Science Foundation under Grant No. CMMI-2137749.

References

[1] J. von Neumann and E. P. Wigner, *Über Merkwürdige Diskrete Eigenwerte*, Collect. Work. Eugene Paul Wigner Part A Sci. Pap. 291 (1993).

[2] C. W. Hsu, B. Zhen, A. D. Stone, J. D. Joannopoulos, and M. Soljačić, *Bound States in the Continuum*, Nat. Rev. Mater. **1**, 16048 (2016).

[3] A. F. Sadreev, *Interference Traps Waves in an Open System: Bound States in the Continuum*, Rep. Prog. Phys. **84**, 055901 (2021).

[4] E. N. Bulgakov and A. F. Sadreev, *Bound States in the Continuum in Photonic Waveguides Inspired by Defects*, Phys. Rev. B **78**, 075105 (2008).

[5] Y. Plotnik, O. Peleg, F. Dreisow, M. Heinrich, S. Nolte, A. Szameit, and M. Segev, *Experimental Observation of Optical Bound States in the Continuum*, Phys. Rev. Lett.

107, 183901 (2011).

[6] M.-S. Hwang, K.-Y. Jeong, J.-P. So, K.-H. Kim, and H.-G. Park, *Nanophotonic Nonlinear and Laser Devices Exploiting Bound States in the Continuum*, Commun. Phys. **5**, 106 (2022).

[7] A. Cerjan, C. Jörg, S. Vaidya, S. Augustine, W. A. Benalcazar, C. W. Hsu, G. von Freymann, and M. C. Rechtsman, *Observation of Bound States in the Continuum Embedded in Symmetry Bandgaps*, Sci. Adv. **7**, eabk1117 (2021).

[8] M. V. Rybin, K. L. Koshelev, Z. F. Sadrieva, K. B. Samusev, A. A. Bogdanov, M. F. Limonov, and Y. S. Kivshar, *High-Q Supercavity Modes in Subwavelength Dielectric Resonators*, Phys. Rev. Lett. **119**, 243901 (2017).

[9] K. Koshelev, G. Favraud, A. Bogdanov, Y. Kivshar, and A. Fratalocchi, *Nonradiating Photonics with Resonant Dielectric Nanostructures*, Nanophotonics **8**, 725 (2019).

[10] Z. Sakotic, A. Krasnok, A. Alú, and N. Jankovic, *Topological Scattering Singularities and Embedded Eigenstates for Polarization Control and Sensing Applications*, Photonics Res. **9**, 1310 (2021).

[11] W. Huang, S. Liu, Y. Cheng, J. Han, S. Yin, and W. Zhang, *Universal Coupled Theory for Metamaterial Bound States in the Continuum*, New J. Phys. **23**, 093017 (2021).

[12] M.-S. Hwang, H.-C. Lee, K.-H. Kim, K.-Y. Jeong, S.-H. Kwon, K. Koshelev, Y. Kivshar, and H.-G. Park, *Ultralow-Threshold Laser Using Super-Bound States in the Continuum*, Nat. Commun. **12**, 4135 (2021).

[13] M. Kang, Z. Zhang, T. Wu, X. Zhang, Q. Xu, A. Krasnok, J. Han, and A. Alù, *Coherent Full Polarization Control Based on Bound States in the Continuum*, Nat. Commun. **13**, 4536 (2022).

[14] A. C. Overvig, S. C. Malek, M. J. Carter, S. Shrestha, and N. Yu, *Selection Rules for Quasibound States in the Continuum*, Phys. Rev. B **102**, 035434 (2020).

[15] E. Davies, *Trapped Modes in Acoustic Waveguides*, Q. J. Mech. Appl. Math. **51**, 477 (1998).

[16] C. M. Linton and P. McIver, *Embedded Trapped Modes in Water Waves and Acoustics*, Wave Motion **45**, 16 (2007).

[17] L. Huang, Y. K. Chiang, S. Huang, C. Shen, F. Deng, Y. Cheng, B. Jia, Y. Li, D. A. Powell, and A. E. Miroshnichenko, *Sound Trapping in an Open Resonator*, Nat. Commun. **12**, 4819 (2021).

[18] L. Huang, B. Jia, Y. K. Chiang, S. Huang, C. Shen, F. Deng, T. Yang, D. A. Powell, Y. Li, and A. E. Miroshnichenko, *Topological Supercavity Resonances in the Finite System*, Adv. Sci. **9**, 2200257 (2022).

[19] M. Tsimokha, V. Igoshin, A. Nikitina, I. Toftul, K. Frizyuk, and M. Petrov, *Acoustic Resonators: Symmetry Classification and Multipolar Content of the Eigenmodes*, Phys. Rev. B **105**, 165311 (2022).

[20] P. McIver and M. McIver, *Trapped Modes in an Axisymmetric Water-Wave Problem*, Q. J. Mech. Appl. Math. **50**, 165 (1997).

[21] P. McIver and M. McIver, *Motion Trapping Structures in the Three-Dimensional Water-Wave Problem*, J. Eng. Math. **58**, 67 (2007).

[22] C. J. Fitzgerald and P. McIver, *Passive Trapped Modes in the Water-Wave Problem for a Floating Structure*, J. Fluid Mech. **657**, 456 (2010).

[23] P. J. Cobelli, V. Pagneux, A. Maurel, and P. Petitjeans, *Experimental Study on Water-Wave Trapped Modes*, J. Fluid Mech. **666**, 445 (2011).

[24] T. Lepetit and B. Kanté, *Controlling Multipolar Radiation with Symmetries for Electromagnetic Bound States in the Continuum*, Phys. Rev. B **90**, 241103 (2014).

[25] D. R. Abujetas, Á. Barreda, F. Moreno, J. J. Sáenz, A. Litman, J.-M. Geffrin, and J. A. Sánchez-Gil, *Brewster Quasi Bound States in the Continuum in All-Dielectric Metasurfaces from Single Magnetic-Dipole Resonance Meta-Atoms*, Sci. Rep. **9**, 16048 (2019).

[26] A. A. Bogdanov, K. L. Koshelev, P. V. Kapitanova, M. V. Rybin, S. A. Gladyshev, Z. F. Sadrieva, K. B. Samusev, Y. S. Kivshar, and M. F. Limonov, *Bound States in the Continuum and Fano Resonances in the Strong Mode Coupling Regime*, Adv. Photonics **1**, 016001 (2019).

[27] Q. Zhou, Y. Fu, L. Huang, Q. Wu, A. Miroshnichenko, L. Gao, and Y. Xu, *Geometry Symmetry-Free and Higher-Order Optical Bound States in the Continuum*, Nat. Commun. **12**, 4390 (2021).

[28] S. Han et al., *All‐ Dielectric Active Terahertz Photonics Driven by Bound States in the Continuum*, Adv. Mater. **31**, 1901921 (2019).

[29] L. Huang et al., *General Framework of Bound States in the Continuum in an Open Acoustic Resonator*, Phys. Rev. Appl. **18**, 054021 (2022).

[30] N. J. J. van Hoof, D. R. Abujetas, S. E. T. ter Huurne, F. Verdelli, G. C. A. Timmermans, J. A. Sánchez-Gil, and J. G. Rivas, *Unveiling the Symmetry Protection of Bound States in the Continuum with Terahertz Near-Field Imaging*, ACS Photonics **8**, 3010 (2021).

[31] S.-G. Lee, S.-H. Kim, and C.-S. Kee, *Bound States in the Continuum (BIC) Accompanied by Avoided Crossings in Leaky-Mode Photonic Lattices*, Nanophotonics **9**, 4373 (2020).

[32] S. Hein, W. Koch, and L. Nannen, *Trapped Modes and Fano Resonances in Two-*

Dimensional Acoustical Duct–Cavity Systems, J. Fluid Mech. **692**, 257 (2012).

[33] D. C. Marinica, A. G. Borisov, and S. V. Shabanov, *Bound States in the Continuum in Photonics*, Phys. Rev. Lett. **100**, 183902 (2008).

[34] F. Wu, C. Fan, K. Zhu, J. Wu, X. Qi, Y. Sun, S. Xiao, H. Jiang, and H. Chen, *Tailoring Electromagnetic Responses in a Coupled-Grating System with Combined Modulation of near-Field and Far-Field Couplings*, Phys. Rev. B **105**, 245417 (2022).

[35] A. S. Pilipchuk and A. F. Sadreev, *Accidental Bound States in the Continuum in an Open Sinai Billiard*, Phys. Lett. A **381**, 720 (2017).

[36] A. A. Lyapina, A. S. Pilipchuk, and A. F. Sadreev, *Trapped Modes in a Non-Axisymmetric Cylindrical Waveguide*, J. Sound Vib. **421**, 48 (2018).

[37] M. S. Sidorenko, O. N. Sergaeva, Z. F. Sadrieva, C. Roques-Carmes, P. S. Muraev, D. N. Maksimov, and A. A. Bogdanov, *Observation of an Accidental Bound State in the Continuum in a Chain of Dielectric Disks*, Phys. Rev. Appl. **15**, 034041 (2021).

[38] Z. F. Sadrieva, I. S. Sinev, K. L. Koshelev, A. Samusev, I. V. Iorsh, O. Takayama, R. Malureanu, A. A. Bogdanov, and A. V. Lavrinenko, *Transition from Optical Bound States in the Continuum to Leaky Resonances: Role of Substrate and Roughness*, ACS Photonics **4**, 723 (2017).

[39] K. Koshelev, A. Bogdanov, and Y. Kivshar, *Meta-Optics and Bound States in the Continuum*, Sci. Bull. **64**, 836 (2019).

[40] J. Jin, X. Yin, L. Ni, M. Soljačić, B. Zhen, and C. Peng, *Topologically Enabled Ultrahigh-Q Guided Resonances Robust to out-of-Plane Scattering*, Nature **574**, 501 (2019).

[41] X. Yin, J. Jin, M. Soljačić, C. Peng, and B. Zhen, *Observation of Topologically Enabled Unidirectional Guided Resonances*, Nature **580**, 467 (2020).

[42] A. Overvig, N. Yu, and A. Alù, *Chiral Quasi-Bound States in the Continuum*, Phys. Rev. Lett. **126**, 073001 (2021).

[43] Y. Chen et al., *Observation of Intrinsic Chiral Bound States in the Continuum*, Nature **613**, 474 (2023).

[44] Z. Zhou, B. Jia, N. Wang, X. Wang, and Y. Li, *Observation of Perfectly-Chiral Exceptional Point via Bound State in the Continuum*, Phys. Rev. Lett. **130**, 116101 (2023).

[45] A. Kodigala, T. Lepetit, Q. Gu, B. Bahari, Y. Fainman, and B. Kanté, *Lasing Action from Photonic Bound States in Continuum*, Nature **541**, 196 (2017).

[46] Y. Yu, A. Sakanas, A. R. Zali, E. Semenova, K. Yvind, and J. Mørk, *Ultra-Coherent Fano Laser Based on a Bound State in the Continuum*, Nat. Photonics **15**, 758 (2021).

[47] S. Huang, T. Liu, Z. Zhou, X. Wang, J. Zhu, and Y. Li, *Extreme Sound Confinement From Quasibound States in the Continuum*, Phys. Rev. Appl. **14**, 021001 (2020).

[48] L. Cao, Y. Zhu, S. Wan, Y. Zeng, Y. Li, and B. Assouar, *Perfect Absorption of Flexural Waves Induced by Bound State in the Continuum*, Extrem. Mech. Lett. **47**, 101364 (2021).

[49] S. Huang, S. Xie, H. Gao, T. Hao, S. Zhang, T. Liu, Y. Li, and J. Zhu, *Acoustic Purcell Effect Induced by Quasibound State in the Continuum*, Fundam. Res. (2022).

[50] D. M. Pozar, *Microwave Engineering* (John Wiley & Sons, 2011).

[51] S. Fan, W. Suh, and J. D. Joannopoulos, *Temporal Coupled-Mode Theory for the Fano Resonance in Optical Resonators*, J. Opt. Soc. Am. A **20**, 569 (2003).

[52] L. Wang, Z. Zhao, M. Du, H. Qin, R. T. Ako, and S. Sriram, *Tuning Symmetry-Protected Quasi Bound State in the Continuum Using Terahertz Meta-Atoms of Rotational and Reflectional Symmetry*, Opt. Express **30**, 23631 (2022).

[53] B. Jia, L. Huang, A. S. Pilipchuk, S. Huang, C. Shen, A. F. Sadreev, Y. Li, and A. E.

Miroshnichenko, *Bound States in the Continuum Protected by Reduced Symmetry of Three-Dimensional Open Acoustic Resonators*, Phys. Rev. Appl. **19**, 054001 (2023).